AFRL-AFOSR-JP-TR-2016-0037

Device Performance and Reliablity Improvements of AlGaBN/GaN/Si MOSFET

Robert Wallace
UNIVERSITY OF TEXAS AT DALLAS

02/04/2016
Final Report

Air Force Research Laboratory
AF Office Of Scientific Research (AFOSR)/ IOA
Arlington, Virginia 22203
Air Force Materiel Command

REPORT DOCUMENTATION PAGE

Form Approved
OMB No. 0704-0188

1. REPORT DATE *(DD-MM-YYYY)*	2. REPORT TYPE	3. DATES COVERED *(From - To)*
04-02-2016	Final	23-06-2014 to 22-12-2015

4. TITLE AND SUBTITLE
Device Performance and Reliablity Improvements of AlGaBN/GaN/Si MOSFET

5a. CONTRACT NUMBER
FA2386-14-1-4069

5b. GRANT NUMBER
Grant 14IOA070_144069

5c. PROGRAM ELEMENT NUMBER
61102F

6. AUTHOR(S)
Robert Wallace

5d. PROJECT NUMBER

5e. TASK NUMBER

5f. WORK UNIT NUMBER

7. PERFORMING ORGANIZATION NAME(S) AND ADDRESS(ES)
UNIVERSITY OF TEXAS AT DALLAS
800 W CAMPBELL RD
RICHARDSON, TX 75080 US

8. PERFORMING ORGANIZATION REPORT NUMBER
N/A

9. SPONSORING/MONITORING AGENCY NAME(S) AND ADDRESS(ES)
AOARD
UNIT 45002
APO AP 96338-5002

10. SPONSOR/MONITOR'S ACRONYM(S)
AFRL/AFOSR/IOA(AOARD)

11. SPONSOR/MONITOR'S REPORT NUMBER(S)
14IOA070_144069

12. DISTRIBUTION/AVAILABILITY STATEMENT
Distribution Code A: Approved for public release, distribution is unlimited.

13. SUPPLEMENTARY NOTES

14. ABSTRACT
A half cycle study of plasma enhanced atomic layer deposited (PEALD) Al2O3 on AlGaN is investigated using in situ X-ray photoelectron spectroscopy, low energy ion scattering, and ex situ electrical characterizations. A faster nucleation or growth is detected from PEALD relative to purely thermal ALD using an H2O precursor. The remote O2 plasma oxidizes the AlGaN surface slightly at the initial stage, which passivates the surface and reduces the OFF-state leakage. This work demonstrates that PEALD is a useful strategy for Al2O3 growth on AlGaN/GaN devices. In addition, unpublished work on AlN films are grown on AlGaN/GaN using PEALD is presented. An AlON interfacial layer is detected at the initial stage, and the interfacial layer may result in a high interface state density. The further optimization of PEALD AlN, especially at the initial stage is necessary in order to passivate the AlGaN/GaN HETMs using the PEALD AlN.

15. SUBJECT TERMS
AlGaN/GaN/Si, nanotechnology, power-efficient system on chip

16. SECURITY CLASSIFICATION OF:			17. LIMITATION OF ABSTRACT	18. NUMBER OF PAGES	19a. NAME OF RESPONSIBLE PERSON
a. REPORT	b. ABSTRACT	c. THIS PAGE			Kenneth Caster
Unclassified	Unclassified	Unclassified	SAR	23	19b. TELEPHONE NUMBER *(Include area code)* +81-42-511-2000

Standard Form 298 (Rev. 8/98)
Prescribed by ANSI Std. Z39.18

Final Annual Report for AOARD Grant FA2386-14-1-4069

Device Performance and Reliability Improvements of AlGaN/GaN/Si MOSFET
US 12 month extension (2014 – 2015) for current Joint Projects

Name of Principal Investigators: Robert M. Wallace

- E-mail address : rmwallace@utdallas.edu
- Institution : University of Texas at Dallas
- Mailing Address : 800 W. Campbell Road, RL10
- Phone : 972-883-6638
- Fax : 972-883-5725

Period of Performance: 23-Jun-2014 to 22-Dec-2015

Executive Summary

This program provided a follow-on extension to FA2386-11-1-4077. A half cycle study of plasma enhanced atomic layer deposited (PEALD) Al_2O_3 on AlGaN is investigated using *in situ* X-ray photoelectron spectroscopy, low energy ion scattering, and *ex situ* electrical characterizations. A faster nucleation or growth is detected from PEALD relative to purely thermal ALD using an H_2O precursor. The remote O_2 plasma oxidizes the AlGaN surface slightly at the initial stage, which passivates the surface and reduces the OFF-state leakage. This work demonstrates that PEALD is a useful strategy for Al_2O_3 growth on AlGaN/GaN devices. The contents of this section are adapted with permission from a paper entitled "In situ plasma enhanced atomic layer deposition half cycle study of Al_2O_3 on AlGaN/GaN high electron mobility transistors" [Applied Physics Letters, 107, 081608, (2015)]. Copyright [2015], AIP Publishing LLC. In addition, unpublished work on AlN films are grown on AlGaN/GaN using PEALD is presented. An AlON interfacial layer is detected at the initial stage. The interfacial layer may result in a high interface state density, D_{it}. The further optimization of PEALD AlN, especially at the initial stage is necessary in order to passivate the AlGaN/GaN HETMs using the PEALD AlN. The work herein was presented at the annual review held in Seoul, S. Korea in October, 26-29, 2015.

Publications during this grant period

[1] X. Qin, L. Cheng, S. McDonnell, A. Azcatl, H. Zhu, J. Kim, and R.M. Wallace, "A comparative study of atomic layer deposition of Al_2O_3 and HfO_2 on AlGaN/GaN" J. Mater. Sci. Mater. Electron. **26**, 4638 (2015).

[2] X. Qin and R.M. Wallace, "In situ plasma enhanced atomic layer deposition half cycle study of Al_2O_3 on AlGaN/GaN high electron mobility transistors " Appl. Phys. Lett. **107**, 081608 (2015).

Section 1: In situ plasma enhanced atomic layer deposition half cycle study of Al_2O_3 on AlGaN/GaN high electron mobility transistors

1.1. Introduction

Metal insulator semiconductor AlGaN /GaN high electron mobility transistors (MISHEMTs) are promising for power device applications due to a lower leakage current than the conventional Schottky AlGaN/GaN HEMTs.[1–3] Among a large number of insulator materials, an Al_2O_3 dielectric layer, deposited by atomic layer deposition (ALD), is often employed as the gate insulator because of a large band gap (and the resultant high conduction band offset on AlGaN[4]), high breakdown field, conformal growth, and a relatively high dielectric constant.[5–7] In the past decade, much work has been done to study the device performance, as well as the interface chemistry for Al_2O_3/AlGaN/GaN MISHEMTs.[5,6,8–17] Although an ALD Al_2O_3 insulator layer grown by Tri-Methyl- Aluminum (TMA) and H_2O precursors decreases the leakage current significantly, the ALD Al_2O_3 is not effective in the passivation of the native AlGaN surface or reduction of the interface state density (D_{it}).[5,12,18] Moreover, due to a high density of positive charges at the AlGaN surface, an undesirable negative threshold voltage shift appears after the ALD Al_2O_3.[6] Recently, numerous reports support that the oxidation of AlGaN can decrease the positive interface charges as well as the D_{it}.[18–25] Our recent work also demonstrates that a remote O_2/N_2 plasma exposure at 550 °C is an available passivation method prior to ALD Al_2O_3.[18] In contrast, O_2 plasma pretreatments under different conditions (flow, time, temperature etc.) may result in surface damage and a threshold voltage instability (ƛV> 1 V).[26] It is well known that plasma enhanced atomic layer deposition (PEALD) can grow an oxide layer using an oxygen plasma to replace the H_2O precursor.[27–29] Recently, work by R.Meunier *et al* shows that PEALD Al_2O_3 is able to enhance device performances.[16,20] However, whether this improvement is relative to the surface oxidation or the Al_2O_3 film is unclear. In this work, a comparison of purely thermal ALD and PEALD is performed to investigate the impact of the O_2 plasma ambient on the AlGaN surface using *in situ* X-ray photoelectron spectroscopy (XPS) and low energy ion scattering (LEIS). *Ex situ* Capacitance-Voltage (C-V) and Current-Voltage (I-V) measurements are exploited to evaluate the associated device performance.

1.2. Experimental

Undoped (0001) $Al_{0.25}Ga_{0.75}N$ samples (30 nm), grown on a 1.2 μm GaN layer on a p-type Si(111) substrate by metal organic chemical vapor deposition (see the wafer structure in Fig. 1.1 (a) in the supplemental material[30]), were obtained from DOWA Electronics Materials (Tokyo, Japan). The samples were first solvent cleaned in acetone, methanol, and

isopropanol for one minute each. These samples were then immediately mounted to a sample plate and introduced into an ultra-high vacuum (UHV) system, described in detail elsewhere,[30] which consists of a number of vacuum chambers interconnected by a UHV transfer tube, maintained at $< 5 \times 10^{-10}$ mbar. This configuration enables the study of *in situ* surface treatments, thin film depositions, and surface characterizations without exposure to atmospheric conditions, preventing spurious surface contamination.

In order to monitor the growth and reaction of Al_2O_3 on the AlGaN surface, XPS was carried out after specific points in the study: (a) after loading the samples to UHV, (b) upon exposing the samples to an atomic layer deposition reactor (Picosun PR200 PEALD reactor (Masala, Finland) operated under purely thermal or plasma-enhanced modes for comparison) for 30 min of annealing (300 °C and 200 °C for ALD and PEALD, respectively, consistent with the following deposition temperature), and (c) after each individual "half cycle"[14,31] pulse of the ALD/PEALD process up to two full cycles. Specifically, the samples were first exposed to one pulse of TMA in the reactor and interrogated with XPS, then transferred back to the PEALD reactor and exposed to one pulse of H_2O (ALD) or remote O_2 plasma (PEALD) prior to again being examined with XPS. The samples were also examined with XPS after 5, 10, 20 and 100 full cycles. *In situ* LEIS was also performed on the sample surface after 20 cycles.

In this study, one full thermal ALD sequence is 0.1 s TMA + 6s Ar Purge + 0.1s H_2O +4s Ar Purge, and the deposition temperature was 300 °C; one full PEALD cycle sequence is 0.1 s TMA + 6 s Ar purge + 28 s remote O_2 plasma + 4 s Ar purge, and the deposition temperature was 200 °C. The remote O_2 plasma was generated by 160 sccm O_2 flow at 2.75 kW. High purity (99.9999%) Ar was used as the precursor carrier and purging gas. The base pressure of the reactor was ~5 mbar.

The XPS was carried out using a monochromated Al kα ($h\nu$ = 1486.7 eV) X-ray source, equipped with a 7 channel analyzer, using a pass energy of 15 eV, with all scans taken at 45° with respect to the sample normal. Spectra were taken of the Ga 2$p_{3/2}$, Ga 3*d*, N 1*s*, Al 2*p*, O 1*s*, and C 1*s* core level regions. XPS peak deconvolution was carried out using an AAnalyzer software with a detailed peak fitting procedure described elsewhere.[14,32] All peaks were referenced to the N 1*s* peak at 397.0 eV to compensate for any shifts in the peak core level positions due to band bending. The LEIS was carried out using the same 7 channel analyzer with biasing conditions suitable for ion detection, and He+ ions excited by an ISE 100 fine focus ion gun using 1 kV bias and 10 mA emission current.

Additional ~1×1 cm^2 AlGaN samples from the same wafer were similarly prepared with subsequent 100 cycles of PEALD Al_2O_3 (for a nominal Al_2O_3 thickness of ~10 nm verified by *ex situ* ellipsometry carried on 100 cycles of Al_2O_3 on Si reference samples) for device

fabrication. The schematic diagrams and geometry details of MOS diodes and transistors are also depicted in Fig. 1.1, which shows a cross section of MISHEMTs and images of MOSCAPs and MOSHEMTs fabricated in this study. C-V measurements were performed on the diodes by an Agilent 4284 LCR meter with a step of 0.2 V and AC modulation voltage of 50 mV with sweep frequencies varying from 5 to 400 kHz. I-V measurements were carried out using a Keithley 4200. All C-V and I-V characterizations were remained in the dark to avoid the influence of photoionization of trapped electrons.[33] The diode fabrication flow for C-V measurements has been described previously.[12,18] For the transistor fabrication, a mesa isolation using 500 s BCl_3 (15 sccm)/Ar (5 sccm) reactive ion etching (RIE) was first processed. The etching depth was ~ 150 nm. Then, ohmic source/drain regions (see Fig. 1.1 (b) and (c)) defined by a standard photolithography were opened by 20 s BCl_3/Ar reactive ion

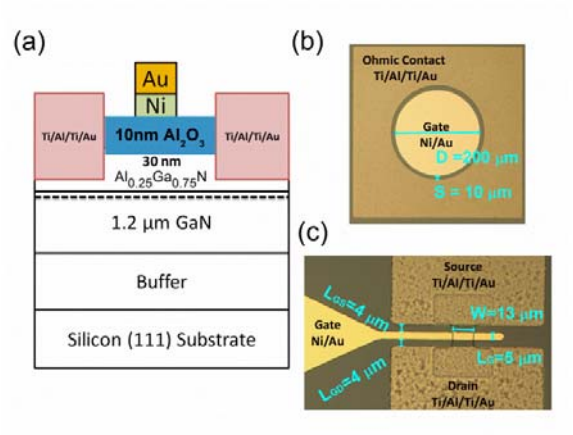

Fig. 1.1. (a) Schematic cross section of MISHEMTs. Optical images of (b) the diode structure for C-V and gate leakage characterizations and, and (c) the transistor structure for I-V characterizations.

etching (removing the Al_2O_3 layer). The ohmic contacts were then formed by e-beam evaporation deposition (base pressure ~1×10^{6} mbar) of Ti/Al/Ti/Au (20 nm/ 40nm/ 20nm/ 100 nm) flowed by rapid thermal annealing at 850 °C for 60 s with 2000 sccm N_2 after patterning by lift off. Gate electrodes defined by the photolithography were finally fabricated using e-beam deposition of Ni/Au (50 nm/100 nm thickness) and lift off.

1.3. Results

The N 1*s* and Ga *LMM* Auger spectra for each individual step in the ALD process are shown in Fig. 1.2 (a). Ga/Al-N bonding (397.0 eV) and Ga $L_2M_{45}M_{45}$ Auger feature (spanning ~392-398 eV) are detected. After 20 cycles of PEALD Al_2O_3, the intensities of N 1*s* and Ga *LMM* decrease by ~65% due to the attenuation of the overlying Al_2O_3 film. In order to understand chemical states of nitrogen clearly, the N *1s* and Ga *LMM* spectra after annealing and after 20 cycles of PEALD Al_2O_3 are shown in Fig. 1.2 (b). There is no evidence of detectable Ga-ON (~ 398 eV) or N-O (~ 402 eV) bonding, which results in undesirable defects on AlGaN according to our previous *in situ* O_2 plasma pretreatment work.[12] The N 1*s*/Ga *LMM* ratio decreases slightly after 20 cycles of Al_2O_3 because of a formation of surface Ga/Al oxide, and will be further discussed in the Ga $2p_{3/2}$ and Al 2*p* spectra below.

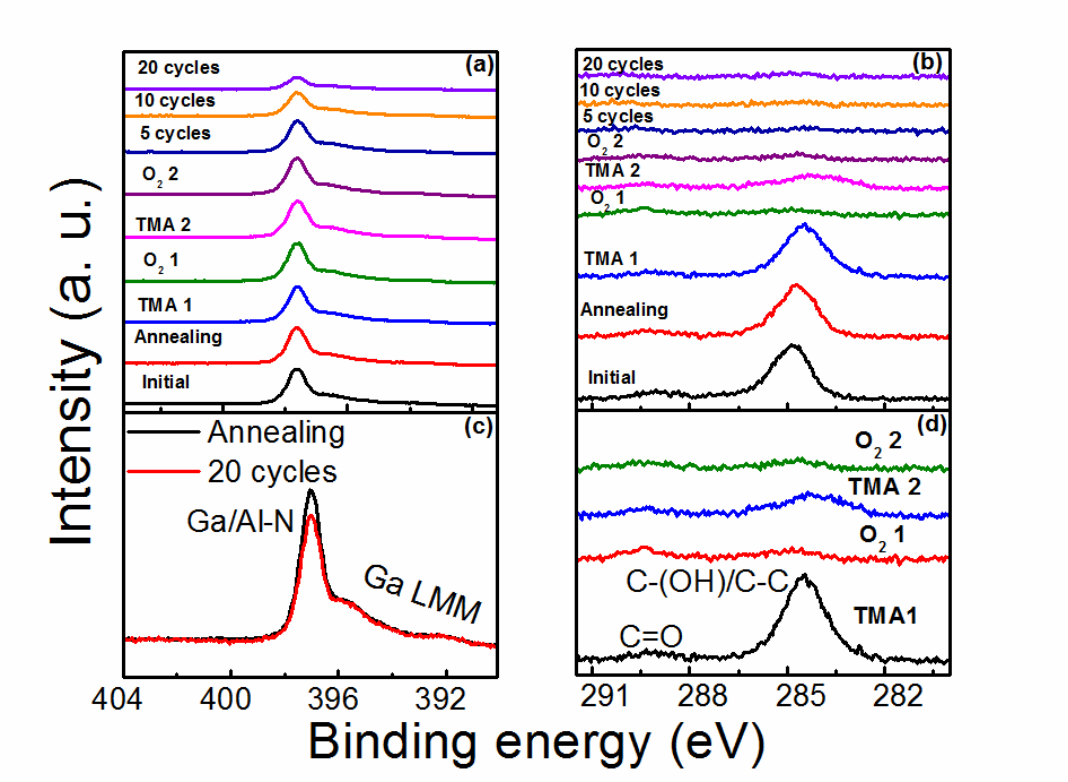

Fig. 1.2. *In situ* XPS spectra of (a) N 1*s*/Ga *LMM* and (c) C 1*s* core levels from the initial surface, after annealing at 200 °C and each ALD half or full cycle, as indicated. (b) N 1*s*/Ga *LMM* spectra normalized to the Ga *LMM* feature after annealing and after 20 cycles of PEALD Al_2O_3. (d) C 1*s* spectra from the first two cycles of PEALD indicating the initial stage of PEALD Al_2O_3 and its impact on AlGaN surface.

The C 1*s* spectra for each individual step are shown in Fig. 1.2 (c). For the initial starting surface, C=O (~290 eV) and C-(O)H/C-C (~284.5 eV) bonds are detected. The *in situ* 200 °C annealing is not effective at removing the carbon concentration, consistent with our previous work.[14,31] In order to observe the initial reaction between the AlGaN surface and TMA/O_2 plasma, the C 1*s* spectra for the first two full ALD cycles (four half cycles) are also shown in Fig. 1.2 (d). After the first pulse of TMA, the carbon concentration does not increase. Upon exposure to the first pulse of the O_2 plasma (28 s), the C 1*s* peaks, especially the C(O)H/C-C concentration, decreases significantly while the intensity of the C=O feature does not change. After the second pulse of TMA, the C 1*s* peak at ~284.5 eV corresponding to Al-CH_3 binding clearly appears. This behavior indicates that the first pulse of O_2 plasma changes the AlGaN surface, which provides nucleation sites for the following TMA precursor. After the second pulse of O_2 plasma, the C 1*s* peaks corresponding to C-H bonds decrease again, suggesting the removal of CH_3 and a full cycle of TMA/O_2 plasma reaction. The carbon concentration after 20 cycles of PEALD is below XPS detection limits, suggesting a complete reaction with minimized carbon incorporation.

Fig. 1.3 (a) presents the normalized and deconvoluted Ga 2$p_{3/2}$ spectra for each individual deposition stage, and shows two peaks indicative of Ga-N bonding from the substrate and Ga-O bonding at the surface. In our work, Ga 2$p_{3/2}$ spectra are commonly used due to the superior surface sensitivity (and signal intensity) of the Ga 2$p_{3/2}$ spectra relative to other Ga spectral peaks produced using the Al Kα (hν = 1486.7 eV) source.[35] The fitting parameters are consistent with our previous reports.[10,12,14,18,31] The ratio of the Ga-O to Ga-N

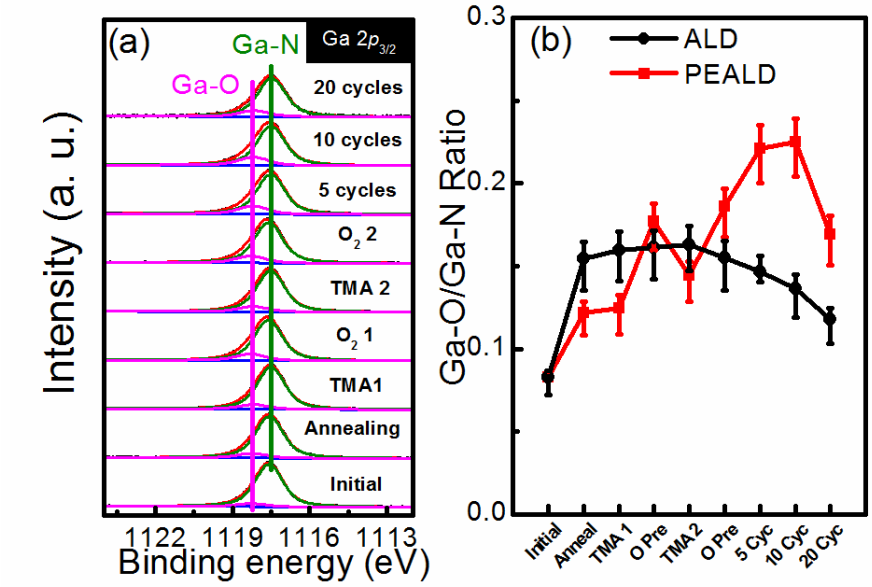

Fig. 1.3. (a) *In situ* XPS spectra of Ga 2$p_{3/2}$ core levels from the initial surface, after annealing in 200 °C and each individual ALD half cycle. (b) The area ratio of Ga-O/Ga-N from Ga 2$p_{3/2}$ shows the change of Ga-oxide concentration during half cycle of ALD and PEALD.

peak area (intensity) for the PEALD Al_2O_3 is plotted in Fig. 1.3 (b). As a reference, the ratio of the Ga-O/Ga-N peak areas for the ALD Al_2O_3 is also plotted in Fig. 1.3 (b). The first pulse of TMA does not change the Ga-O concentration. An obvious increase of Ga-oxide is detected after the first pulse of O_2 plasma, but not after the first H_2O precursor as shown in Fig. 1.3 (b). This indicates that the remote plasma oxygen exposure oxidizes the AlGaN surface. Upon exposure to the second pulse of TMA, the Ga-O peak decrease is likely due to the formation Ga-O-Al bonding at the surface.[10] The final Ga-O/Ga-N intensity ratios are ~11.7±1.5% and 16.9±1.9% for ALD and PEALD Al_2O_3, respectively. If we assume that the surface oxide layer consists of 75 % Ga_2O_3 and 25% Al_2O_3, the thickness of the Ga/Al oxide layers after 20 cycles of ALD Al_2O_3 and PEALD are both less than 0.1 nm based on the intensity attenuation of the N 1*s* peak, which is below the monolayer (~0.26 nm) coverage. In summary, the PEALD process slightly increases the oxide concentration at the surface relative to the ALD process.

The Al 2*p* spectra for each individual stage in PEALD are shown in Fig. 1.4 (a), which is a direct monitor of the growth of Al_2O_3. The ratio of Al-O to Al-N during the half cycle EALD is shown in Fig. 1.4 (b) and the ratio of the Al-O/Al-N for each stage during ALD of

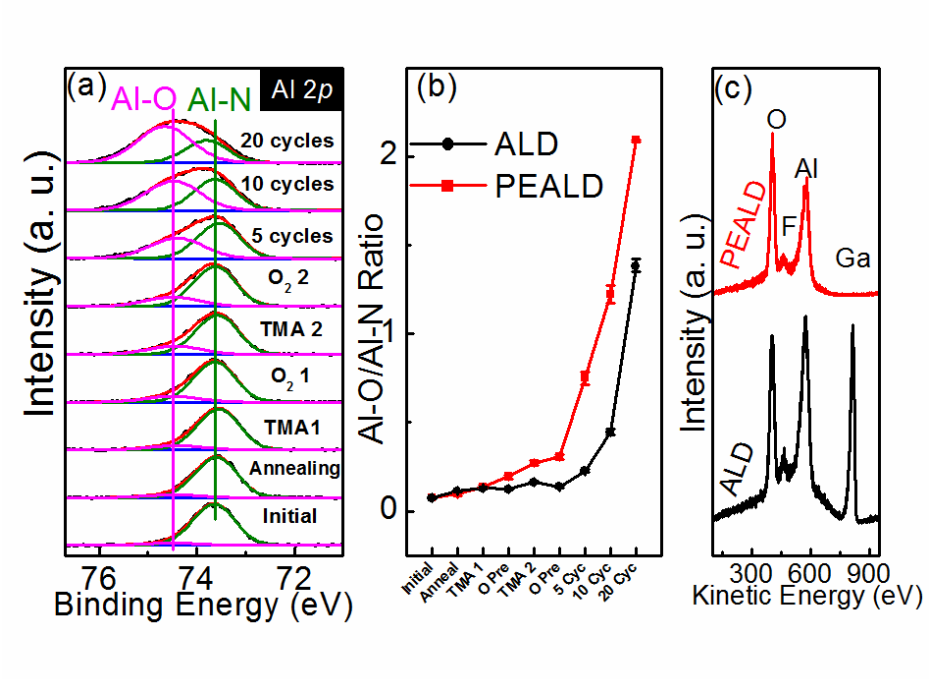

Fig. 1.4. (a) *In situ* XPS spectra of Al 2*p* core levels from initial surface, after annealing in 200 °C and each individual ALD half cycle. (b) The ratio of Al-O/Al-N from Al 2*p* peaks during half cycle ALD and PEALD indicating the growth of Al_2O_3. (c) Comparison of LEIS after 20 cycles of ALD to the PEALD Al_2O_3 studied here. (see 25 cycles of ALD Al_2O_3 on AlGaN in ref. 10)

Al_2O_3 is also shown. The detection of the Al-N bulk peak at 73.5 eV, as well as Al_2O_3 at 74.4 eV, is noted.[14,31] Due to the low binding energy of Al 2*p* core level, the intensity of Al-O bond from the substrate is less prominent compared to the detection of Ga-O from the surface sensitive Ga $2p_{3/2}$ core level.[4,10,12,14,18,31] Consistent with Ga $2p_{3/2}$ spectra, the Al-O bond increases slightly after annealing and the first pulse of O_2 plasma. Importantly, the intensity ratio for PEALD increases faster than the ALD process, indicating the nucleation or growth of PEALD Al_2O_3 on AlGaN is more facile than ALD. It should be noted that measured Al_2O_3 growth rates on Si substrate for ALD and PEALD are 1.14±0.01 and 1.13±0.01 Å/cycles, respectively, suggesting that the difference of growth rates could be ignored here. The thickness of the PEALD Al_2O_3 after 20 cycles on AlGaN is ~ 1.4 nm according to the attenuation of Ga $2p_{3/2}$ peak area. In contrast, the thickness of ALD Al_2O_3 is ~1.0 nm after 20 cycles. Thus, the relatively enhanced growth is due to Ga/Al-oxide formation (which are reactive nucleation sites for the TMA precursor) after the O_2 plasma exposure, likely coupled with the removal of carbon contamination, which may mitigate the reaction between the AlGaN surface and the TMA precursor.[10] Additionally, a much better coverage of Al_2O_3 by PEALD is demonstrated by *in situ* LEIS, which is sensitive to only the outmost exposed atomic layers on the surface.[35] As Fig. 1.4 (c) shows, no Ga peak is detected while an obvious Ga peak (815 eV) is found with 20 cycles of ALD Al_2O_3 on AlGaN, suggesting that the PEALD Al_2O_3 results in the complete coverage at the initial stage. Moreover, the higher Al peak from the ALD Al_2O_3 sample relative to the PEALD Al_2O_3 is also due to the uncovered AlGaN surface.

The stoichiometry of the ALD Al_2O_3 and the PEALD is the same within detectable limits. as seen in Fig. 1.5. The detection of a small fluorine (F) peak is noted and is due to decomposition of reactor elastomer seals. The concentration of F is below XPS detection

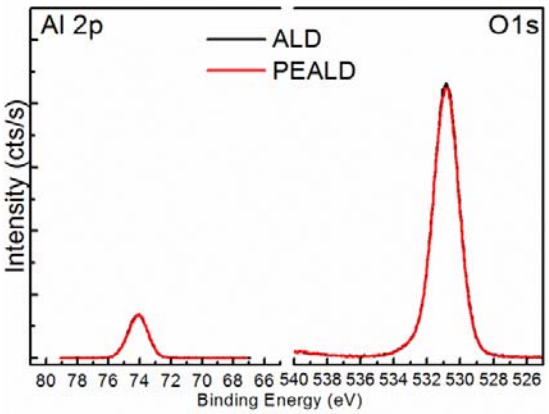

Fig. 1.5. XPS of Al 2p and O 1s core level spectra from 100 cycles of ALD Al_2O_3 and 100 cycles of PEALD Al_2O_3, respectively. The spectra are indistinguishable.

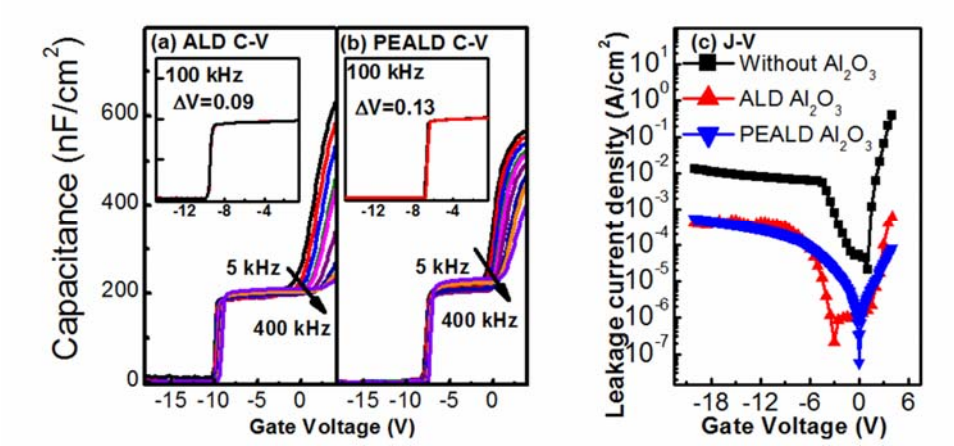

Fig. 1.6. (Color online) Comparison of frequency-dependent C-V curves for (a) ALD Al_2O_3/ AlGaN/GaN and (b) PEALD Al_2O_3/AlGaN/GaN diodes. Insets show forward and backward C-V curves. (c) Leakage current density-voltage plots for shottky AlGaN/GaN, ALD Al_2O_3/AlGaN/GaN and PEALD Al_2O_3/AlGaN/GaN diodes.

limits and does not affect the discussion here.

The frequency-dependent C-V curves from 5 kHz to 400 kHz at room temperature are measured to evaluate the interface quality. These C-V curves from diode structures incorporating ALD Al_2O_3 and PEALD Al_2O_3 dielectric layers are shown in Fig. 1.6 (a) and (b), and reveal a standard two-step C-V feature.[12,18] Capacitance values for diodes at the plateau where the two dimension electron gas (2DEG) forms are 194 and 196 nF/cm^2 for ALD and PEALD, respectively, consistent with the ~10 nm Al_2O_3/AlGaN stack capacitance.[4] Obvious frequency dependence of capacitance dispersion is detected for both diodes upon further gate bias, corresponding to a high D_{it}. Here, "border trap" (trap states inside the gate insulator but close to the interface), should be not key sources of the D_{it} at the Al_2O_3/AlGaN interface. Our previous work demonstrates that Al_2O_3/AlGaN and HfO_2/AlGaN diodes present a similar level of D_{it}, and AlGaN surfaces have a much more impact on the D_{it}. R.D. Long *et al*. also show the absence of border traps for ALD Al_2O_3/GaN interface.[36] The PEALD approach decreases the dispersion slightly. This may be due to the formation of Ga-O, which likely passivates the AlGaN surface.[18] The forward and backward C-V curves at 100 kHz can be seen as insets within Fig. 1.6 (a) and (b), and show very small hysteresis values (ƛV): 0.09 and 0.13 V for ALD and PEALD Al_2O_3, respectively. It is thought that the PEALD process does not contribute a significant density of slow traps.[12] The gate leakage current densities of Schottky AlGaN/GaN, ALD Al_2O_3/AlGaN/GaN, and PEALD Al_2O_3/AlGaN/GaN

are shown in Fig 1.6. (c).

Fig. 1.7 (a) and (d) show the O 1*s* core level spectra along with the onset of the O loss features upon 100 cycles of Al_2O_3 on AlGaN. The band gap of the Al_2O_3 films can be extracted from the separation between the O 1*s* core level feature and the onset of its loss feature originated from the excitation of electrons from the valence band to the conduction band.[37,38] As Fig. 1.7 (a) and (d) show, the extracted ALD and PEALD Al_2O_3 band gap values are both 6.9±0.1 eV. The valence band spectra offset (VBO) values between the AlGaN surface and then after 100 cycles of ALD and 100 cycles of PEALD Al_2O_3 are determined to be 1.2±0.1 and 1.1±0.1 eV, respectively. The deduced conduction band offset (CBO) values for ALD Al_2O_3/AlGaN and PEALD Al_2O_3/AlGaN are 1.8 and 1.9 eV, respectively.

Either ALD or PEALD Al_2O_3 layer effectively suppresses the leakage current, consistent with the relatively high conduction band offset (CBO) values in the band diagram (see Fig. 1.7 (c) and (f)). It should be noted that the O_2 plasma in the PEALD is well controlled using a relative short exposure time (28 s/per pulse) and a low substrate temperature (200 °C). In contrast, our previous work shows that a 10 min of 300 °C O_2 plasma exited by another RF plasma generator results in an worse frequency dispersion than ALD Al_2O_3/AlGaN/GaN diodes.[18] Therefore, it is essential to control and optimize the O_2 plasma conditions for a specific tool carefully.

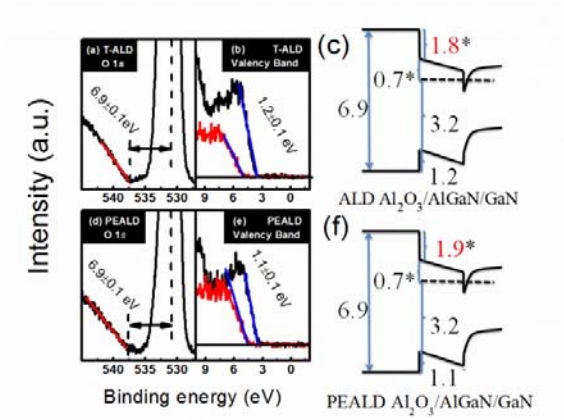

Fig.1.7 XPS of O 1*s* core level spectra showing the onset of O loss features for 100 cycles of (a) ALD Al_2O_3/AlGaN and (d) PEALD Al_2O_3/AlGaN, XPS valence band spectra for AlGaN and 100 cycles of (b) ALD Al_2O_3/AlGaN and (e) PEALD Al_2O_3/AlGaN, and energy band diagram for (c) ALD Al_2O_3/AlGaN/GaN and (f) PEALD Al_2O_3/AlGaN/GaN interfaces.

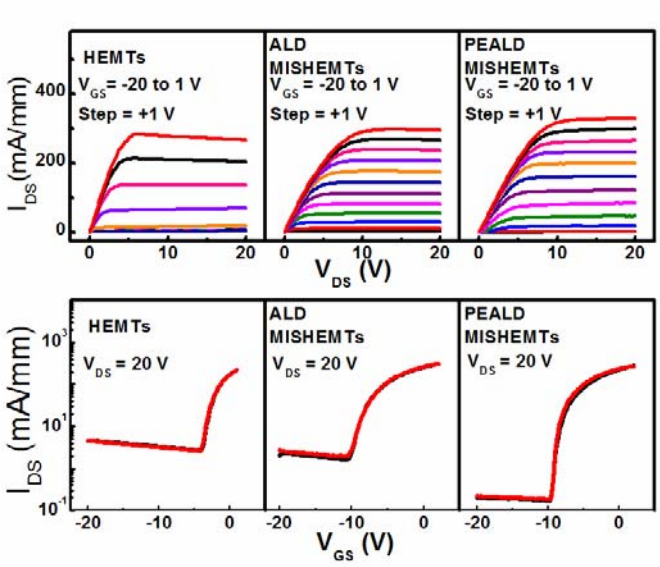

Fig. 1.8. (a) Output characteristics of HEMTs, ALD-MISHEMTs and PEALD-MISHEMTs. (b) Transfer characteristics of HEMTs, ALD-MISHEMTs and PEALD-MISHEMTs indicating a lower OFF-state leakage.

The threshold voltage (V_{TH}) values extracted from I_{DS}-V_{DS} curves are -3.9, -10.3, and -9.5 V for HEMTs, ALD-MOSHEMTs, and PEALD-MOSHEMTs, respectively, and the extrapolation methods are included in the Appendix 1. Obviously, a negative V_{TH} shift is detected from MISHEMTs with Al_2O_3 layer due to a high density of positive charges at the interface, in agreement with our previous work.[4] However, compared to ALD-MISHEMTs, there is a +1 V V_{TH} shift for PEALD-MISHEMTs. The oxidation of AlGaN during PEALD Al_2O_3 likely reduces the positive charge density.[18] The DC characteristics of HEMT and MISHEMTs are plotted in Fig. 1.8 (a). The I_{DS}-V_{DS} output characteristics for all devices present a standard pinch off behavior. The saturation forward and backward I_{DS}-V_{GS} at V_{DS} = 20 V curves are shown in Fig. 1.8 (b). Importantly, the PEALD Al_2O_3 layer reduces the OFF-state drain leakage by more than one order of magnitude and improves the I_{ON}/I_{OFF} current ratio. This behavior also reveals that the chemical control of the interface is also critical for the transistor transfer performance. Consistent with the C-V response, no obvious V_{TH} instability is detected.

1.4. Conclusion

In conclusion, a high quality Al_2O_3 film is grown on AlGaN/GaN using PEALD, with the faster nucleation rate and better coverage than that obtained through standard, thermal

ALD. The remote plasma conditions in the PEALD process result in a slight increase of Al/Ga oxide without formation of Ga/Al-O-N or N-O bonding. According to our previous studies, the formation Ga-O-N but not Ga-O is a sign of device degradation.[12,18] The Al/Ga-oxide passivates the AlGaN surface and decreases D_{it} as well as the OFF-state leakage. As expected, the PEALD Al_2O_3 layer reduces the gate leakage current, similar to ALD Al_2O_3. Overall, PEALD Al_2O_3 is an appropriate technology for the Al_2O_3 growth on AlGaN.

Section 1 References

[1] T. Hashizume, S. Ootomo, S. Oyama, M. Konishi, and H. Hasegawa, J. Vac. Sci. Technol. B **19**, 1675 (2001).

[2] M.A. Khan, X. Hu, a. Tarakji, G. Simin, J. Yang, R. Gaska, and M.S. Shur, Appl. Phys. Lett. **77**, 1339 (2000).

[3] U.K. Mishra, P. Parikh, and Y.F. Wu, Proc. IEEE **90**, 1022 (2002).

[4] X. Qin, L. Cheng, S. McDonnell, A. Azcatl, H. Zhu, J. Kim, and R.M. Wallace, J. Mater. Sci. Mater. Electron. **26**, 4638 (2015).

[5] S. Yang, Z. Tang, K. Wong, Y. Lin, C. Liu, Y. Lu, S. Huang, and K.J. Chen, IEEE Electron Device Lett. **34**, 1497 (2013).

[6] M. Ťapajna, M. Jurkovič, L. Válik, Š. Haščík, D. Gregušová, F. Brunner, E.-M. Cho, T. Hashizume, and J. Kuzmík, J. Appl. Phys. **116**, 104501 (2014).

[7] G.D. Wilk, R.M. Wallace, and J.M. Anthony, J. Appl. Phys. **89**, 5243 (2001).

[8] T. Hashizume, S. Anantathanasarn, N. Negoro, E. Sano, H. Hasegawa, K. Kumakura, and T. Makimoto, Jpn. J. Appl. Phys. **43**, L777 (2004).

[9] M. Capriotti, A. Alexewicz, C. Fleury, M. Gavagnin, O. Bethge, D. Visalli, J. Derluyn, H.D. Wanzenböck, E. Bertagnolli, D. Pogany, and G. Strasser, Appl. Phys. Lett. **104**, 113502 (2014).

[10] X. Qin, H. Dong, B. Brennan, A. Azacatl, J. Kim, and R.M. Wallace, Appl. Phys. Lett. **103**, 221604 (2013).

[11] M. Van Hove, X. Kang, S. Stoffels, D. Wellekens, N. Ronchi, R. Venegas, K. Geens, and S. Decoutere, IEEE Trans. Electron Devices **60**, 3071 (2013).

[12] X. Qin, A. Lucero, A. Azcatl, J. Kim, and R.M. Wallace, Appl. Phys. Lett. **105**, 011602 (2014).

[13] X.-H. Ma, J.-J. Zhu, X.-Y. Liao, T. Yue, W.-W. Chen, and Y. Hao, Appl. Phys. Lett. **103**, 033510 (2013).

[14] B. Brennan, X. Qin, H. Dong, J. Kim, and R.M. Wallace, Appl. Phys. Lett. **101**, 211604 (2012).

[15] R. Lossy, H. Gargouri, M. Arens, and J. Würfl, J. Vac. Sci. Technol. A **31**, 01A140 (2013).

[16] R. Meunier, A. Torres, and M. Charles, ECS Trans. **58**, 269 (2013).

[17] K.-Y. Park, H.-I. Cho, J.-H. Lee, S.-B. Bae, C.-M. Jeon, J.-L. Lee, D.-Y. Kim, C.-S. Lee, and J.-H. Lee, Phys. Status Solidi **7**, 2351 (2003).

[18] X. Qin, H. Dong, J. Kim, and R.M. Wallace, Appl. Phys. Lett. **105**, 141604 (2014).

[19] H.-Y. Liu, C.-S. Lee, W.-C. Hsu, L.-Y. Tseng, B.-Y. Chou, C.-S. Ho, and C.-L. Wu, IEEE Trans. Electron Devices **60**, 2231 (2013).
[20] R. Meunier, a. Torres, E. Morvan, M. Charles, P. Gaud, and F. Morancho, Microelectron. Eng. **109**, 378 (2013).
[21] N. Harada, Y. Hori, N. Azumaishi, K. Ohi, and T. Hashizume, Appl. Phys. Express **4**, 021002 (2011).
[22] F. Roccaforte, F. Giannazzo, F. Iucolano, C. Bongiorno, and V. Raineri, J. Appl. Phys. **106**, 023703 (2009).
[23] S. Huang, X. Liu, K. Wei, G. Liu, X. Wang, B. Sun, X. Yang, B. Shen, C. Liu, S. Liu, M. Hua, S. Yang, and K.J. Chen, Appl. Phys. Lett. **106**, 033507 (2015).
[24] D. Gregušová, M. Jurkovič, Š. Haščík, M. Blaho, a. Seifertová, J. Fedor, M. Ťapajna, K. Fröhlich, P. Vogrinčič, J. Liday, J. Derluyn, M. Germain, and J. Kuzmik, Appl. Phys. Lett. **104**, 013506 (2014).
[25] L.-H. Huang, S.-H. Yeh, C.-T. Lee, H. Tang, J. Bardwell, and J.B. Webb, IEEE Electron Device Lett. **29**, 284 (2008).
[26] S. Ozaki, T. Ohki, M. Kanamura, T. Imada, N. Nakamura, N. Okamoto, T. Miyajima, and T. Kikkawa, Int. Conf. Compd. Semicond. Manuf. Technol. Digest, Boston, MA 23-26 Apric 2012, paper 11a.1, availabe at http://gaasmantech.com/Digest/2012/papers/11a.1.087.pdf.
[27] S.M. George, Chem. Rev. **110**, 111 (2010).
[28] B. Hoex, S.B.S. Heil, E. Langereis, M.C.M. Van De Banden, and W.M.M. Kessels, Appl. Phys. Lett. **89**, 3 (2006).
[29] J.W. Lim and S.J. Yun, Electrochem. Solid-State Lett. **7**, F45 (2004).
[30] R.M. Wallace, ECS Trans. **16**, 255 (2008).
[31] X. Qin, B. Brennan, H. Dong, J. Kim, C.L. Hinkle, and R.M. Wallace, J. Appl. Phys. **113**, 244102 (2013).
[32] A. Herrera-Gómez, A. Hegedus, and P.L. Meissner, Appl. Phys. Lett. **81**, 1014 (2002).
[33] O. Ueda and S.J. Pearton, editors , in *Materials and Reliability Handbood for Semiconuctor Optical and Electron Devices* (Springer,New York, 2013), pp. 147–205.
[34] C.L. Hinkle, M. Milojevic, E.M. Vogel, and R.M. Wallace, Appl. Phys. Lett. **95**, 151905 (2009).
[35] F. Zhang, B. King, and D. O'connor, Phys. Rev. Lett. **75**, 4646 (1995).
[36] R.D. Long, A. Hazeghi, M. Gunji, Y. Nishi, and P.C. McIntyre, Appl. Phys. Lett. **101**, 241606 (2012).
[37] X. Qin, L. Cheng, S. McDonnell, A. Azcatl, H. Zhu, J. Kim, and R.M. Wallace, J. Mater. Sci. Mater. Electron. **26**, 4638 (2015).
[38] F. Bell and L. Ley, Phys. Rev. B **37**, 8383 (1988)

Section 2: *In situ plasma enhanced atomic layer deposition study of AlN on AlGaN/GaN high electron mobility transistors*

2.1. Introduction

AlN, with high thermal conductivity, wide direct band gap (Eg = 6.2 eV), high electrical resistant, high fusion temperature and high chemical stability, extends the application of the III-nitride to high temperature and high power. Moreover, because of the close lattice constants and thermal properties of AlN and GaN, AlN is typically used as a buffer layer for GaN-based devices where low defect structures are needed. Recently, AlN as the dielectric layer on AlGaN/GaN HEMTs emerge as another compelling candidate.[1–4] A very effective AlN passivation technique featuring an AlN prepared by plasma enhanced atomic layer deposition (PEALD) has been demonstrated to deliver low current collapse and high breakdown voltage.[4] In our study, we investigate the growth and impact of PEALD AlN on AlGaN using *in situ* XPS.

2.2. Experimental

Undoped (0001) $Al_{0.25}Ga_{0.75}N$ samples (30 nm), grown on a 1.2 μm GaN layer on a Si(111) substrate by metal organic chemical vapor deposition (the same wafer in the previous PEALD Al_2O_3 experiment), were used in this study. The samples were first solvent cleaned in acetone, methanol, and isopropanol for one minute each. These samples were then immediately mounted to a sample plate and introduced into the ultra-high vacuum (UHV) system that was introduced in Section 1. In order to monitor the growth of AlN on the AlGaN surface, XPS was carried out after loading the sample to the UHV system, upon exposing the samples to the PEALD chamber, and after 10, 20, 50 and 100 full cycles. In this study, one full PEALD cycle sequence is 0.1 s TMA + 6 s Ar purge + 40 s remote forming gas (FG) plasma + 4 s Ar purge, and the deposition temperature was 250 °C. The remote FG plasma was generated by 160 sccm FG (95% N_2/5% H_2) flow at 2 kW. High purity (99.9999%) Ar was used as the precursor carrier and purging gas. The base pressure of the reactor was ~5 mbar. The XPS was carried out to collect spectra of the Ga 2$p_{3/2}$, Ga 3*d*, N 1*s*, Al 2*p*, O 1*s*, and C 1*s* core level regions. XPS peak deconvolution was carried out using the AAnalyzer software. And all peaks were referenced to the N 1*s* peak at 397.0 eV to compensate for any shifts in the peak core level positions due to band bending.

Additional ~1×1 cm^2 AlGaN samples from the same wafer were similarly prepared with subsequent 100 cycles of PEALD AlN for device fabrication. The fabrication process, the schematic diagrams and geometry details of MOS diodes are the same as that presented in Section 1. C-V measurements were again characterized by the Agilent 4284 LCR meter with sweep frequencies varying from 1 kHz to 1MHz.

2.3. Results

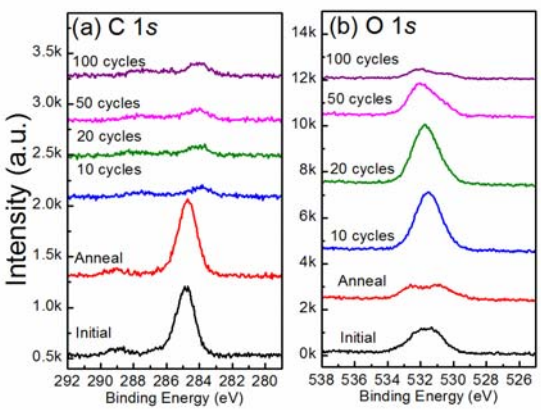

Fig. 2.1 *In situ* XPS spectra of (a) C 1*s* and (b) O 1*s* core levels from the initial surface, after annealing and PEALD AlN.

The C 1*s* spectra for each step are shown in Fig. 2.1 (a). Consistent with our previous work,[5–7] the *in situ* annealing is not effective at the removal of the carbon from the initial starting surface. However, the carbon concentration decreases by 80% after 10 cycles of AlN. In our previous *in situ* study, the XPS results have revealed that N_2 and FG plasma both facilitate removal of carbon contamination.[7] Upon to the 100 cycles, where all carbon signals come from AlN film, a low concentration of carbon is detected. Fig. 2.1(b) presents the O 1*s* spectra for the each stage. Obviously, the annealing reduces the oxygen slightly. However, the oxygen increases significantly after 10 cycles of TMA/FG. Actually, 500 cycles of AlN was done on Si wafer to reduce the carbon and oxygen contamination in the chamber before depositing AlN on AlGaN/GaN samples. And the XPS results from the AlN film on Si samples indicate a low carbon (2%) and oxygen (3%). Carbon and oxygen contaminations as the notorious issue in PEALD AlN have been investigated by many researchers.[8–11] The carbon contamination is caused by residual TMA precursor molecules that have not been removed completely during the FG plasma step. The integration of oxygen in the film is due to the strong hydrophilic behavior of the TMA precursor. Since the PEALD chamber conditions don't change, oxygen adsorbates from the sample plate (4 inches round Mo plate) are possible sources at the initial stage.

N 1*s* and Ga *LMM* Auger spectra for each step are shown in Fig. 2.2. N-Ga/Al peaks at 397.0 eV and Ga $L_2M_{45}M_{45}$ Auger feature spanned ~392-398 eV are detected at the initial stage and after the annealing. After 10 cycles of TMA/FG, an additional feature at ~398 eV is detected, which should be corresponding to CN_x[7] and Al-ON peaks. And it is consistent with the change of C 1*s* and O 1*s* in Fig. 2.1. After 50 and 100 cycles of TMA/FG, the features at 398 eV have the higher intensities than 10 and 20 cycles of TMA/FG due to the generation of NH_x, which will be further discussed in the Al 2*p* spectra (see Fig. 2.4). After 100 cycles of

TMA/FG, the Ga $L_2M_{45}M_{45}$ Auger peaks are below XPS detection limitations. Thus, it is reasonable to claim that the primary peak at 397 eV after 100 cycles of TMA/FG is the Al-N from PEALD AlN film.

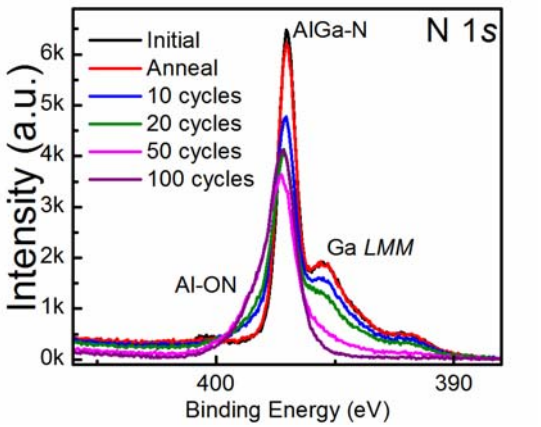

Fig. 2.2 *In situ* XPS spectra of N 1*s* core levels from the initial surface, after annealing and PEALD AlN.

The raw spectra of Ga $2p_{3/2}$ are shown in Fig. 2.3(a). With the increase of deposition cycles, the intensity of Ga $2p_{3/2}$ decreases due to the attenuation of PEALD AlN film. After 100 cycles of AlN, the Ga $2p_{3/2}$ is already below the XPS detection limitations. The Fig. 2.3(b) presents the normalized and deconvoluted Ga $2p_{3/2}$ spectra that show two peaks indicative Ga-N bonding from the substrate and Ga-O at the AlGaN surface or AlN/AlGaN interfaces. After the annealing, the Ga-O concentration increase due to the transfer of oxygen from C-O.[5–7] No significant changes are detected after the deposition of AlN.

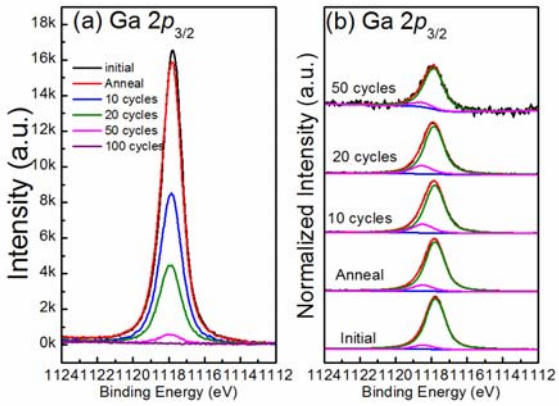

Fig. 2.3 *In situ* XPS spectra of (a) raw Ga $2p_{3/2}$ and (b) normalized fitted Ga $2p_{3/2}$ core levels from the initial surface, after annealing and PEALD AlN.

Fitted Al 2*p* spectra are shown in Fig. 2.4. After 10 cycles of TMA/FG, an obvious Al-O/Al-ON peak at 74.6 eV is observed and this peak keeps increasing upon to 20 cycles. It is consistent with the trend of oxygen in Fig. 2.1(b). It indicates that the AlON is preferable at the initial nucleation. After 50 cycles, an Al-N peak at 73.9 eV from PEALD AlN is detected

with Al-O/Al-ON and attenuated Al-N (from AlGaN substrate) peaks. While a small Al-O/Al-ON peak is still detectable at the higher binding energy, the primary peak is Al-N from PEALD Al-N film after 100 cycles of TMA/FG. Here, the Al-O/Al-ON signal is from AlN film but not the interfacial layer since the AlN is thick enough to block the interfacial or substrate signals that have been proven in Ga $L_2M_{45}M_{45}$ (see Fig. 2.2) and Ga 2*p* (see Fig.2.3 (a)) spectra. In contrast, the features at 398 eV in N 1*s* core levels in Fig. 2.2 increase after 100 cycles of TMA/FG. Since this increase doesn't originate from Al-ON or CN_X, it is reasonable to deduce that it is from NH_X. A certain amount of hydrogen contamination due to the organic TMA precursor and FG plasma has been observed using Fourier transform infrared spectroscopy (FTIR) characterizations.[12]

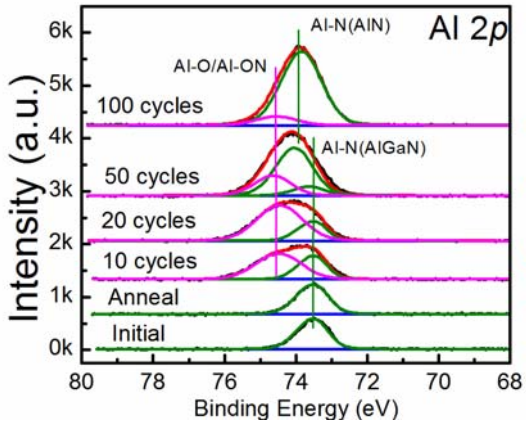

Fig. 2.4 *In situ* XPS spectra of (a) raw Ga $2p_{3/2}$ and (b) normalized and fitted Ga $2p_{3/2}$ core levels from the initial surface, after annealing and PEALD AlN.

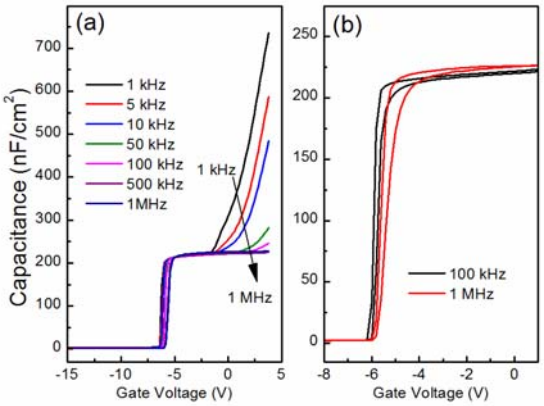

Fig. 2.5 (a) frequency-dependent C-V curves and (b) forward and backward C-V curves at 100 kHz and 1MHz for PEALD AlN/AlGaN/GaN diodes.

The frequency-dependent C-V curves from 1 kHz to 1 MHz at room temperature are measured and shown in Fig. 2.5(a). Obvious frequency dependence of capacitance dispersion is observed upon further gate bias, corresponding to a high D_{it}. It suggests that the PEALD AlN could not passivate the AlGaN surface as PEALD Al_2O_3. It is likely due to the AlON

interfacial layer at the initial stage. We have demonstrated that GaON results in a high D_{it} in our previous work. The AlON might have a similar effect with the GaON. Fig. 2.5 (b) shows hysteresis values at 100 kHz and 1 MHz, which are higher than 300 mV. The higher hysteresis could originate from the interface as well as the AlN film.

2.4. Conclusion

In conclusion, an AlN film is grown on AlGaN/GaN using PEALD. An AlON interfacial layer is detected at the initial stage. After 50 cycles of TMA/FG, a typical AlN with low carbon and oxygen contamination is formed. The interfacial layer may result in a high D_{it}. The optimization of PEALD AlN, especially at the initial stage, is necessary in order to passivate the AlGaN/GaN HETMs using the PEALD AlN. For example, an *in situ* plasma pretreatment prior to PEALD AlN is possible approach to reduce the high oxygen contamination at the initial growth.

Section 2 References

[1] Y. Lu, Q. Jiang, Z. Tang, S. Yang, C. Liu, and K.J. Chen, Appl. Phys. Express **8**, 064101 (2015).

[2] S. Huang, Q. Jiang, and S. Yang, IEEE Electron Device Lett. **34**, 2012 (2013).

[3] A. Koehler, N. Nepal, T. Anderson, D. Hobart, C. Eddy, and F. Kub, IEEE Electron Device Lett. **34**, 1115 (2013).

[4] S. Huang, Q. Jiang, and S. Yang, IEEE Electron Device Lett. **33**, 516 (2012).

[5] B. Brennan, X. Qin, H. Dong, J. Kim, and R.M. Wallace, Appl. Phys. Lett. **101**, 211604 (2012).

[6] X. Qin, B. Brennan, H. Dong, J. Kim, C.L. Hinkle, and R.M. Wallace, J. Appl. Phys. **113**, 244102 (2013).

[7] X. Qin, H. Dong, B. Brennan, A. Azacatl, J. Kim, and R.M. Wallace, Appl. Phys. Lett. **103**, 221604 (2013).

[8] S. Goerke, M. Ziegler, A. Ihring, J. Dellith, A. Undisz, M. Diegel, S. Anders, U. Huebner, M. Rettenmayr, and H.-G. Meyer, Appl. Surf. Sci. **338**, 35 (2015).

[9] H. Van Bui, F.B. Wiggers, A. Gupta, M.D. Nguyen, A. a. I. Aarnink, M.P. de Jong, and A.Y. Kovalgin, J. Vac. Sci. Technol. A Vacuum, Surfaces, Film. **33**, 01A111 (2015).

[10] P. Motamedi and K. Cadien, Appl. Surf. Sci. **315**, 104 (2014).

[11] Y.-C. Perng, T. Kim, and J.P. Chang, Appl. Surf. Sci. **314**, 1047 (2014).

[12] A.P. Perros, H. Hakola, T. Sajavaara, T. Huhtio, and H. Lipsanen, J. Phys. D. Appl. Phys. **46**, 505502 (2013).

Appendix 1

The Extraction of Threshold Voltage

In general, the mathematic model is similar to metal-oxide-semiconductor field-effect-transistors (MOSFETs). (For example, see: S.M.Sze and K. K.Ng, Physics of Semiconductor Devices, 3th ed. (John Wiley & Sons, Inc., Hoboken, New Jersey, 2007).

(1) Linear Extraction

With the gate voltage larger than threshold voltage (V_{TH}), the charge sheet induced by the gate is given by:

$$Q_n = C_o(V_G - V_{TH}) \quad (1)$$

where C_o is the insulator (Al_2O_3 and AlGaN) capacitance, and V_G is the gate bias voltage. When a drain bias is applied, the channel has a variable potential with distance. Therefore, the channel charges as a function of position could be described by equation (2), and the channel current is given by equation (3):

$$Q_{n(x)} = C_o(V_G - V_{TH} - V_x) \quad (2)$$

$$I_D = \frac{Z}{L}\left(\int_0^L Q_{n(x)}\, v(x)dx\right) \quad (3)$$

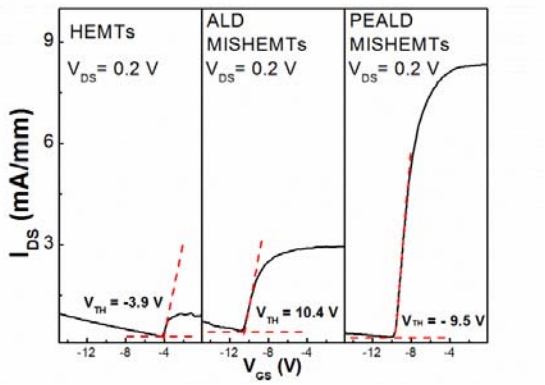

Fig. A. DC I_{DS}-V_{GS} characteristics of HEMTs, ALD-MISHEMTs, and PEALD-MISHEMTs at VDS = 0.2 V

Assuming that the mobility is constant, the drift velocity is given by equation (4) and the drain current as a function of gate voltage at a low drain voltage is given by equation (5).

$$v(x) = \mu_n E(x) = \mu_n \frac{dV_x}{dx} \quad (4)$$

$$I_{DS} = \frac{Z\mu_n C_o}{L}\left[(V_G - V_{TH})V_D - \frac{V_D^2}{2}\right] \quad (5)$$

In the linear region, (VD « (V_G-V_{TH})), equation (5) is reduced to equation (6)

$$I_{DS} = \frac{Z\mu_n C_o}{L}\left[(V_G - V_{TH})V_D\right] \quad (6)$$

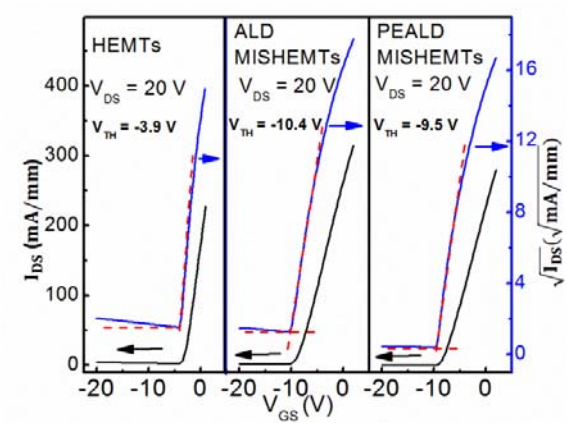

Fig. B. DC I_{DS}-V_{GS} characteristics of HEMTs, ALD-MISHEMTs and PEALD-MISHEMTs at V_{DS} = 20 V.

Therefore, a linear extraction could be performed from Fig. A (V_{DS} = 0.2 V) and the V_{TH} values are -3.9, 10.4 and -9.5 V for HEMTs, ALD-MISHEMTs, and PEALD-MISHEMTs, respectively.

(2) Saturation Current Method

At a high V_{DS}, corresponding to the pinch-off condition, the current saturates are depicted by equation (7)

$$I_{DS} = \frac{Z\mu_n C_o}{L} [(V_G - V_{TH})^2] \quad (7)$$

Therefore, $\sqrt{I_{DS}}$ is linear to V_G, and V_{TH} could be extracted at the onset of I_{DS}-V_{DS} plots as shown in Fig. B. The values are consistent with the values using the linear extraction metho

THIS PAGE LEFT BLANK